# Bounds on the complex permittivity of sea ice

K. Golden

Department of Mathematics, University of Utah, Salt Lake City

**Abstract.** An analytic method for obtaining bounds on effective properties of composites is applied to the complex permittivity $\epsilon^*$ of sea ice. The sea ice is assumed to be a two-component random medium consisting of pure ice of permittivity $\epsilon_1$ and brine of permittivity $\epsilon_2$. The method exploits the properties of $\epsilon^*$ as an analytic function of the ratio $\epsilon_1/\epsilon_2$. Two types of bounds on $\epsilon^*$ are obtained. The first bound $R_1$ is a region in the complex $\epsilon^*$ plane which assumes only that the relative volume fractions $p_1$ and $p_2 = 1 - p_1$ of the ice and brine are known. The region $R_1$ is bounded by circular arcs and $\epsilon^*$ for any microgeometry with the given volume fractions must lie inside it. In addition to the volume fractions, the second bound $R_2$ assumes that the sea ice is statistically isotropic within the horizontal plane. The region $R_2$ is again bounded by circular arcs and lies inside $R_1$. Built into the method is a systematic way of obtaining tighter bounds on $\epsilon^*$ by incorporating information about the correlation functions of the brine inclusions. The bounding method developed here, which does not assume any specific geometry for the brine inclusions, offers an alternative to the classical mixing formula approach adopted previously in the study of sea ice. In these mixing formulas, specific assumptions are made about the inclusion geometry, which are simply not satisfied by the sea ice under many conditions. The bounds $R_1$ and $R_2$ are compared with experimental data obtained from artificially grown sea ice at the frequencies 4.8 and 9.5 GHz. Excellent agreement with the data is achieved.

## 1. Introduction

The remote sensing of sea ice generates many interesting technical and theoretical problems. A central question in the application of remote sensing techniques to studying sea ice is how the physical microstructure of the ice determines its scattering and effective electromagnetic properties. This question plays a fundamental role in correctly interpreting scattering data and images from sea ice. The determination of the electromagnetic properties from microstructural information is particularly interesting in the case of sea ice, which is a complex random medium consisting of pure ice with brine and air inclusions. The details of the microstructure, namely the geometry and relative volume of the inclusions, depend strongly on the temperature of the ice, the conditions under which the ice was grown, and the history of the sample under consideration, as discussed by *Weeks and Ackley* [1982]. Owing to the

wide variety of possible microstructures and the high dielectric contrast of the components, it is, in general, quite difficult to accurately predict the effective complex permittivity of sea ice. Nevertheless, many models have been proposed to describe the dielectric behavior of sea ice, such as those of *Addison* [1969], *Hoekstra and Capillino* [1971], *Stogryn* [1985], *Tinga et al.* [1973], *Vant et al.* [1978], *Golden and Ackley* [1981], *Sihvola and Kong* [1988]. Typically, the sea ice is assumed to consist of a host medium (pure ice) containing spherical or ellipsoidal inclusions (brine or air). Various effective medium theories, such as the coherent potential approximation, have been used to derive "mixing formulas" for the effective permittivity $\epsilon^*$ of the system. Each formula is judged according to how well it predicts experimental data.

While mixing formulas for $\epsilon^*$ are certainly useful, their applicability to the full range of microstructures presented by sea ice is limited. For example, as sea ice warms up to around $-5°C$, the brine pockets tend to coalesce or "percolate" and form a connected matrix of brine, in which case the sea ice becomes a porous medium. This process represents an important stage in the evolution of a sea ice sheet, as it precedes the phenomenon known as "brine rejection," where some

of the brine flows out of the sea ice, due to its porosity. The electromagnetic properties of the ice following the rejection are dramatically changed. Clearly the assumption that the brine (or air) component of sea ice is contained in individual ellipsoidal inclusions, is simply not satisfied when the brine forms a connected matrix. We must therefore question the validity of these mixing formulas for warm ice.

Another limitation of mixing formulas is that they provide only a precise prediction of what $\epsilon^*$ should be, given, say, a value for the brine volume and perhaps some information about the distribution of ellipsoidal orientations, as considered by *Sihvola and Kong* [1988]. They do not provide any information on the range of reasonable values for $\epsilon^*$, which would be very useful, given that in any experiment, as one measures $\epsilon^*$ for a variety of samples, one obtains a scatter of values in the $\epsilon^*$ plane, which may or may not coincide with the precise value predicted by the mixing formula.

We remark that one of the principal motivating factors behind this work is the goal of developing practical electromagnetic methods of distinguishing sea ice types, such as first-year from multiyear ice. In typical inverse scattering algorithms, what is reconstructed from scattered electromagnetic field data is the complex permittivity which is "seen" by the wave. When the wavelength is longer than the microstructural scale, which for sea ice would correspond to frequencies of less than 10 or 20 GHz, this reconstructed permittivity will be $\epsilon^*$, the effective permittivity. (Of course, $\epsilon^*$ itself can vary throughout any given sea ice sheet as the microstructural geometry, such as brine volume, changes through the sheet.) One of our principal goals here is to study in detail how the statistical properties of the sea ice microstructure are connected to these observed values of $\epsilon^*$.

We also remark that another motivation for our study of sea ice is that from the point of view of the mathematical theory of composite materials, understanding the electromagnetic behavior of sea ice pushes the limits of currently available mathematical techniques. From this point of view, sea ice is an extremely interesting example of a composite material, which combines in one medium many of the challenges encountered in the development of the mathematical theory; it is a multicomponent composite, whose components have highly contrasting properties characterized by complex parameters and whose microstructure exhibits a wide range of geometries. In particular, one of the most mathematically intriguing aspects of the microstructure is the coalescing or percolation of the brine cells, which occurs around the critical temperature $T_c \approx -5°C$, and results in a microstructural transition from separated brine pockets to a connected brine matrix. The influence of the connectedness properties of composite microstructures on bulk electromagnetic behavior has been a topic of considerable recent mathematical interest. For ex-

ample, see *Kozlov* [1989], *Golden* [1990], *Golden* [1992], *Golden* [1994], *Berlyand and Golden* [1994], *Bruno* [1991] and K. Golden [Statistical mechanics of conducting phase transitions, submitted to J. Math. Phys., 1995]. It is interesting to note in this context that the connectedness properties of a particular component dominate the behavior of many technologically important materials, including doped semiconductors, porous media (e.g., sandstones), piezocomposites, thermistors, solid rocket propellants, and cermets.

## 2. Description of Theory and Methods

Owing to the above limitations in the mixing formula approach which are caused by the wide variety of relevant sea ice microstructures, we begin here a new approach to studying the effective complex permittivity $\epsilon^*$ of sea ice by obtaining bounds on $\epsilon^*$ in the complex plane. As a first step in the development of this approach, we consider the sea ice to be a two-component random medium consisting of pure ice of complex permittivity $\epsilon_1$ in the volume fraction $p_1$ and brine of complex permittivity $\epsilon_2$ in the volume fraction $p_2 = 1 - p_1$. In this paper we will neglect the effects of air inclusions, which is a reasonable assumption in many situations, such as for first year ice which has not yet undergone brine rejection, where air can replace much of the brine. To obtain the bounds, we apply a method introduced independently by *Bergman* [1978] and *Milton* [1979] which exploits the properties of $\epsilon^*$ as an analytic function of the ratio $\epsilon_1/\epsilon_2$. The method was developed further and applied in various settings by both Bergman and Milton, and the complex bounds used here were obtained independently by *Milton* [1981] and *Bergman* [1980]. A mathematical formulation of the method was given by *Golden and Papanicolaou* [1983] and some of its implications were explored by *Milton and Golden* [1985].

The key step in this formulation is establishing an integral representation for $\epsilon^*$, which is then used to obtain the bounds. As in the case of typical mixing formulas, the bounds are derived in the quasi-static limit, so that they are valid when the wavelength is long compared to the scale of the inhomogeneities.

We now describe the bounds more precisely. For the simplest bound it is assumed that only $\epsilon_1$, $\epsilon_2$, $p_1$, and $p_2$ are known. The bound consists of a lens-shaped region in the complex $\epsilon^*$ plane in which the values of $\epsilon^*$ for all possible mixtures of the two materials in the given volume fractions must lie. For the case of sea ice, where there is a wide variety of possible microstructures, the bound is valid for all of them, given only the brine volume. Built into the method, though, is a systematic way of obtaining tighter bounds on $\epsilon^*$ if one knows further statistical information about the geometry beyond simply the volume fractions. More precisely, there is a hierarchy of increasingly tighter bounds, where the nth order bound depends on knowledge of the $n$-point cor-

relation function of the mixture. The bounds described above are first order and depend only on one–point correlation or volume fraction information. For the case of second-order bounds it turns out that if the material is statistically isotropic, i.e., if $\epsilon^*$ does not depend on the direction of polarization of the electric field, then one can obtain the bounds without any direct knowledge of the two–point correlation function.

In the present work we apply the first order and isotropic second order bounds to sea ice with given salinities and temperatures. These bounds are compared with the experimental data of *Arcone et al.* [1986] for artificially grown sea ice at 4.8 and 9.5 GHz. Given a sample of sea ice at temperature $T$ and of salinity $S$, we estimate the brine volume $p_2$ using the equation of *Frankenstein and Garner* [1967]. Then for each frequency, 4.8 and 9.5 GHz, and for a given temperature $T$, we find the complex permittivity of the brine $\epsilon_2$ using the calculations of *Stogryn and Desargant* [1985]. In general, we obtain excellent agreement with the experimental data. Small discrepancies between the bounds and the real data are inevitable, though, and may be explained with uncertainties in the brine volumes, the unaccounted for presence of air, or scattering effects when the wavelength is larger but comparable to the typical brine length scale.

## 3. Bounds on the Effective Permittivity

We now present the bounds on $\epsilon^*$ discussed above. In this section we first formulate the effective permittivity problem, briefly describe the method for obtaining the bounds, which is called the analytic continuation method, and then state the bounds. A more detailed summary of the method is given in the appendix. We also refer the interested reader to *Golden and Papanicolaou* [1983], *Golden* [1986] and *Bergman* [1982] for more detail.

Let us begin by formulating the effective complex permittivity problem for a two-component random medium in all of $\mathbb{R}^d$, $d$-dimensional Euclidean space, with translation invariant statistics. Formulating the problem in this way is for mathematical simplicity but is analogous to assuming that the brine statistics are the same throughout a given sample of sea ice and that the sample is large compared to the typical brine length scale, which is reasonable for comparison with data taken for samples by *Arcone et al.* [1986]. For real sea ice the brine statistics and structure will change with depth and might differ from floe to floe. However, for a relatively small depth interval of, say, 10 cm, and in any given floe the assumption should be reasonably well satisfied. Now let $\epsilon(\mathbf{x}, \omega)$ be a (spatially) stationary random field in $\mathbf{x} \in \mathbb{R}^d$ and $\omega \in \Omega$, where $\Omega$ is the set of all realizations of our random medium. (We are dealing here with an ensemble $\Omega$ of random media, indexed by the parameter $\omega$, which represents one particular

realization and not frequency.) For a two–component medium with component permittivities $\epsilon_1$ (ice) and $\epsilon_2$ (brine) we write

$$\epsilon(\mathbf{x}, \omega) = \epsilon_1 \chi_1(\mathbf{x}, \omega) + \epsilon_2 \chi_2(\mathbf{x}, \omega), \quad (1)$$

where $\chi_j$ is the characteristic function of medium $j = 1, 2$, which equals one for all realizations $\omega \in \Omega$ having medium $j$ at $\mathbf{x}$, and equals zero otherwise. Let $\mathbf{E}(\mathbf{x}, \omega)$ and $\mathbf{D}(\mathbf{x}, \omega)$ be the stationary random electric and displacement fields, respectively, satisfying

$$\mathbf{D}(\mathbf{x}, \omega) = \epsilon(\mathbf{x}, \omega)\mathbf{E}(\mathbf{x}, \omega) \quad (2)$$

$$\nabla \cdot \mathbf{D}(\mathbf{x}, \omega) = 0 \quad (3)$$

$$\nabla \times \mathbf{E}(\mathbf{x}, \omega) = 0 \quad (4)$$

$$< \mathbf{E}(\mathbf{x}, \omega) > = \mathbf{e}_k, \quad (5)$$

where $\mathbf{e}_k$ is a unit vector in the kth direction, for some $k = 1, \ldots, d$. In (5), angle brackets mean ensemble average over $\Omega$ or spatial average over all of $\mathbb{R}^d$.

In view of the local constitutive law (2) we define the effective complex dielectric tensor $\epsilon^*$ via

$$< \mathbf{D} > = \epsilon^* < \mathbf{E} >, \quad k = 1, \ldots, d, \quad (6)$$

or,

$$\epsilon_{ik}^* = < D_i >, \quad i, k = 1, \ldots d, \quad (7)$$

where the right side of (7) depends on $k$ via (2) and (5). For simplicity we focus on one diagonal coefficient $\epsilon^* = \epsilon_{kk}^*$. Noting that through the homogeneity property $\epsilon^*(\lambda\epsilon_1, \lambda\epsilon_2) = \lambda\epsilon^*(\epsilon_1, \epsilon_2)$, $\epsilon^*$ depends only on the ratio $h = \epsilon_1/\epsilon_2$, we may divide (7) by $\epsilon_2$ and define

$$m(h) = \frac{\epsilon^*}{\epsilon_2} = < (h\chi_1 + \chi_2)E_k >, \quad h = \frac{\epsilon_1}{\epsilon_2}. \quad (8)$$

The two main properties of $m(h)$ are that it is analytic off the interval $(-\infty, 0]$ in the $h$ plane and that it maps the upper half plane to the upper half plane, i.e. ,

$$Im(m(h)) > 0, \qquad Im(h) > 0, \quad (9)$$

where $Im$ denotes imaginary part. Such functions which are analytic off some segment of the real axis and obey (9) are called Herglotz functions.

As mentioned in section 2, the key step in the analytic continuation method is obtaining an integral representation for $\epsilon^*$. For this purpose it is more convenient to look at the function

$$F(s) = 1 - m(h), \quad s = 1/(1 - h), \quad (10)$$

which is analytic off $[0, 1]$ in the $s$ plane. It was then proven by *Golden and Papanicolaou* [1983] that $F(s)$ has the following representation

$$F(s) = \int_0^1 \frac{d\mu(z)}{s - z}, \quad (11)$$

where $\mu$ is a positive measure on $[0, 1]$. (Very loosely

speaking, we may think of $d\mu(z)$ as $g(z)dz$, for some density $g(z)$ which is allowed to have "$\delta$ function" components.) One of the most important features of (11) is that it separates the parameter information in $s = 1/(1 - \epsilon_1/\epsilon_2)$ from information about the geometry of the mixture, which is all contained in $\mu$, through dependence on $\chi_1$. In fact, statistical information about the geometry is input into (11) via the moments of $\mu$,

$$\mu_n = \int_0^1 z^n d\mu(z). \qquad (12)$$

This input is obtained by equating an expansion of (11) in powers of $1/s$, the coefficients of which are the moments $\mu_n$, to a corresponding perturbation expansion around a homogeneous medium ($s = \infty$ or $\epsilon_1 = \epsilon_2$) of another representation for $F(s)$ involving a resolvent formula for $\mathbf{E}$. This procedure, which is described in the appendix, yields

$$\mu_0 = p_1, \qquad (13)$$

if only the volume fractions are known, and

$$\mu_1 = \frac{p_1 p_2}{d} \qquad (14)$$

if the material is statistically isotropic, where $d$ is the dimension of the system as in 6 and (7). In general, knowledge of the $(n + 1)$–point correlation function of the medium allows calculation of $\mu_n$ (in principle).

Bounds on $\epsilon^*$ or $F(s)$ are obtained by fixing $s$ in (11), varying over admissible measures $\mu$ (or admissible geometries), such as those that satisfy only (13), and finding the corresponding range of values of $F(s)$. This procedure is described in the appendix. We now give formulas for the boundaries of these regions. In addition to the first- and second–order bounds described in the Introduction, there are zeroth order bounds which assume no knowledge of the geometry, not even the volume fractions. They exploit only the conditions that $0 \leq \mu_0 \leq 1$ and $F(s = 1) \leq 1$. In the $F$ plane, let $R_0$ be the region containing the range of values of $F(s)$. Then $R_0$ is bounded by a circular arc $C(\alpha)$ and a line segment $L(\alpha)$,

$$C(\alpha) = \frac{\alpha}{s - (1 - \alpha)}, \quad L(\alpha) = \frac{\alpha}{s}, \quad 0 \leq \alpha \leq 1. \quad (15)$$

The arc $C(\alpha)$ is circular because as a function of $\alpha$, $C(\alpha)$ is a fractional linear transformation of $\alpha$, which maps the class of circles and lines to itself. When $s$ is complex, then the line segment $[0, 1]$ in the $\alpha$ plane gets mapped to an arc of a circle. If we transform $R_0$ to the $\epsilon^*$ plane, then its vertices are $\epsilon_1$ and $\epsilon_2$, $L(\alpha)$ gets transformed to the line segment

$$L^*(\alpha) = \alpha\epsilon_1 + (1 - \alpha)\epsilon_2, \quad 0 \leq \alpha \leq 1, \quad (16)$$

and $C(\alpha)$ gets transformed to the circular arc

$$C^*(\alpha) = \left( \frac{\alpha}{\epsilon_1} + \frac{1 - \alpha}{\epsilon_2} \right)^{-1}, \qquad 0 \leq \alpha \leq 1, \quad (17)$$

so that $\alpha$ plays the role of $p_1$, the volume fraction of medium 1. In fact, the expressions in (16) and (17) are simply the complex permittivities of laminates (or layers) of $\epsilon_1$ and $\epsilon_2$ in the relative volume fractions $\alpha$ and $1 - \alpha$ with the applied field parallel and perpendicular, respectively, to the lamination direction. The arc and line segment are parameterized by the relative volume fraction $\alpha$ of $\epsilon_1$. Because there are actual geometries (laminates) which attain these complex bounds, the bounds are said to be optimal, in other words, with no assumptions at all about the geometry, these are the best bounds one can obtain. For real parameters with $\epsilon_1 \leq \epsilon_2$, $R_0$ collapses to the interval

$$\epsilon_1 \leq \epsilon^* \leq \epsilon_2. \qquad (18)$$

If the volume fractions $p_1$ and $p_2 = 1 - p_1$ are known, then (13) must be satisfied. Let $R_1$ be the corresponding region, which is bounded by circular arcs. In the $F$ plane one of these arcs is parameterized by

$$C_1(z) = \frac{p_1}{s - z}, \qquad 0 \leq z \leq p_2, \quad (19)$$

where $z$ is a real parameter and $C(z)$ is fractional linear in $z$, like $C(\alpha)$ above. To exhibit the other arc, it is convenient to consider the auxiliary function

$$E(s) = 1 - \frac{\epsilon_1}{\epsilon^*} = \frac{1 - sF(s)}{s[1 - F(s)]}, \qquad (20)$$

which is a Herglotz function like $F(s)$, analytic off $[0, 1]$. Then in the $E$ plane, we can parameterize the other circular boundary of $R_1$ by

$$\hat{C}_1(z) = \frac{p_2}{s - z}, \qquad 0 \leq z \leq p_1. \quad (21)$$

In the $\epsilon^*$ plane, $R_1$ has vertices $p_1\epsilon_1 + p_2\epsilon_2$ and $(p_1/\epsilon_1 + p_2/\epsilon_2)^{-1}$ and is bounded by the arcs

$$C_1^*(\beta) = \epsilon_2 + p_1 \left/ \left( \frac{1}{\epsilon_1 - \epsilon_2} + \frac{\beta p_2}{\epsilon_2} \right) \right.,$$
$$0 \leq \beta \leq 1, \qquad (22)$$

$$\hat{C}_1^*(\beta) = \epsilon_1 + p_2 \left/ \left( \frac{1}{\epsilon_2 - \epsilon_1} + \frac{\beta p_1}{\epsilon_1} \right) \right.,$$
$$0 \leq \beta \leq 1, \qquad (23)$$

where $\beta$ is a real parameter and $C_1^*(\beta)$ and $\hat{C}_1^*(\beta)$ are again fractional linear in $\beta$. Again, these bounds are optimal and are attained by a number of geometries, including coated elliptical cylinders considered by *Milton* [1981]. When $\epsilon_1$ and $\epsilon_2$ are real, $R_1$ collapses to the interval

$$(p_1/\epsilon_1 + p_2/\epsilon_2)^{-1} \leq \epsilon^* \leq p_1\epsilon_1 + p_2\epsilon_2, \quad (24)$$

which are the classical arithmetic and harmonic mean bounds.

If the material is further assumed to be statistically isotropic, i.e., $\epsilon_{ik}^* = \epsilon^* \delta_{ik}$, then (14) must be satisfied as well. The corresponding region $R_2$, again, has circular arcs for boundaries. In the $F$ plane one of these arcs is parameterized by

$$C_2(z) = \frac{p_1(s-z)}{s(s-z-p_1/d)}, \quad 0 \leq z \leq (d-1)/d. \quad (25)$$

In the $E$ plane the other arc is parameterized by

$$\hat{C}_2(z) = \frac{p_2(s-z)}{s[s-z-p_1(d-1)/d]}, \quad 0 \leq z \leq 1/d. \quad (26)$$

When $\epsilon_1$ and $\epsilon_2$ are real with $\epsilon_1 \leq \epsilon_2$, $R_2$ collapses to the interval

$$\epsilon_1 + p_2 \Big/ \left( \frac{1}{\epsilon_2 - \epsilon_1} + \frac{p_1}{d\epsilon_1} \right) \leq$$
$$\epsilon^* \leq \epsilon_2 + p_1 \Big/ \left( \frac{1}{\epsilon_1 - \epsilon_2} + \frac{p_2}{d\epsilon_2} \right), \quad (27)$$

which are the famous bounds of *Hashin and Shtrikman* [1962]. The real bounds in (27) are attainable by coated sphere geometries, but the complex arcs (25) and (26) are not generally attainable, as noted by *Milton* [1981] and *Bergman* [1982].

## 4. Comparison With Experimental Data

In this section we consider plots of the bounds $R_0, R_1$, and $R_2$ and compare them with the experimental data of *Arcone et al.* [1986]. For any given sample of sea ice of salinity $S$ and temperature $T$ the brine volume $p_2$ may be estimated using the equation of *Frankenstein and Garner* [1967],

$$p_2 = S \left( \frac{49.185}{T} + 0.532 \right). \quad (28)$$

To determine $\epsilon_2$, the complex permittivity of the brine, we use the empirically determined formulas of *Stogryn and Desargant* [1985], which are based on a Debye-type relaxation equation,

$$\epsilon_2 = \epsilon_\infty + \frac{\epsilon_s - \epsilon_\infty}{1 - i2\pi f\tau} + i\frac{\sigma}{2\pi\epsilon_0 f}, \quad (29)$$

which has only one resonance, ignoring a possible spread in relaxation times. In (29), $\epsilon_s$ and $\epsilon_\infty$ are the limiting static and high frequency values of the real part of $\epsilon_2$, $Re(\epsilon_2)$, $\tau$ is the relaxation time, $f$ is the frequency, $\sigma$ is the ionic conductivity of the dissolved salts, $\epsilon_0$ is the permittivity of free space, and $i = (-1)^{1/2}$. The ionic conductivity is assumed to be independent of frequency. Then $\epsilon_2$ for brine in equilibrium with sea ice is determined by the four real parameters $\epsilon_\infty, \epsilon_s, \tau$, and $\sigma$, each of which depends only on temperature, and all were

found experimentally. Compared to the brine, the complex permittivity of the pure ice $\epsilon_1$ is basically independent of temperature and frequency, as found by *Mätzler and Wegmüller* [1987], and we take $\epsilon_1 = 3.15 + i0.002$.

In Figure 1 we plot the bound $R_0$ with $R_1$ contained inside, with the frequency, $S, T$, and $p_2$ values shown. Clearly, knowing the brine volume ($R_1$) yields a tremendous improvement over the $R_0$ bound, which only assumes knowledge of the values of $\epsilon_1$ and $\epsilon_2$. In Figure 2 we have plotted two different regions $R_1$ for the same sample of sea ice with $S = 5^0/_{00}$, to show how changing the temperature shifts the region in the $\epsilon^*$ plane. Alternatively, we can view Figure 2 as showing how changing the brine volume can dramatically affect the location and size of $R_1$. In Figure 3 we have plotted the smaller $R_1$ with $T = -11°C$ from Figure 2 with $R_2$ inside of it. For the calculation of $R_2$ here and in subsequent figures, whose boundaries are given by (25) and (26), we have used $d = 2$, since as the wave propagates vertically down through a slab which is not too thick, the properties are reasonably uniform in this direction. In this case the electric field only has components within the horizontal plane, so that the system is effectively two-dimensional. The assumption of isotropy in this configuration, which is the configuration used by *Arcone et al.* [1986], is then an assumption about isotropy within the horizontal plane, which is a topic considered by *Cherepanov* [1971], *Kovacs and Morey* [1978], *Weeks and Gow* [1980] and *Golden and Ackley* [1981]. (We remark that since the scales on the $Re(\epsilon^*)$ and $Im(\epsilon^*)$ axes are not the same, the circular arcs which form the boundaries of the regions may not necessarily appear circular.)

In Figures 4a, 4b, and 4c we begin the comparison of our bounds with the measured values of $\epsilon^*$ for artificially grown sea ice of *Arcone et al.* [1986]. The data points in Figure 4a were taken from *Arcone et al.* [1986], Figure 8. They represent a range of $p_2$ values from 0.031 to 0.041, and salinity values from $3.8^0/_{00}$ to $4.4^0/_{00}$. To construct the bound, we have chosen the midpoint values of $p_2 = 0.036$ and $S = 4.1^{\ 0}/_{00}$, and then inverted (28) to obtain $T = -6°C$. The data points in Figure 4b range in $p_2$ values from 0.018 to 0.023, with the same salinity range as in Figure 4a, and we obtain the bound through the same midpoint procedure. In Figure 4c, the data have been taken from the 85-4 slab measurements of *Arcone et al.* [1986], Figure 17, with a range in temperature from $-12.5°C$ to $-15.5°C$, so that we choose the midpoint $T = -14°C$, with $S = 2.4^0/_{00}$, to construct the bound. We chose this particular slab because there was little difference between the measured salinity before and after the experiments were done, so that we were fairly confident that the $p_2$ value given by (28) would be representative of what was in the sample. By comparison of the data with $R_2$, there appears to be some evidence of a small degree of anisotropy, which agrees with what was found directly by *Arcone et al.* [1986]. However, these dis-
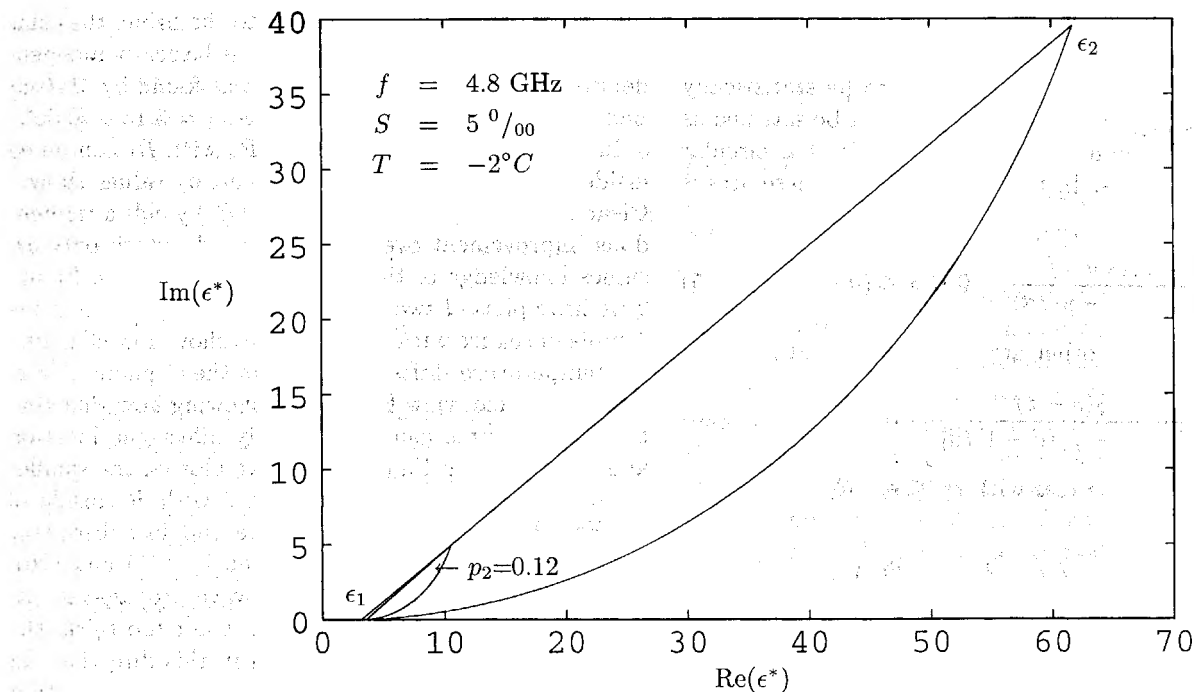
**Figure 1.** Bounds on complex permittivity $\epsilon^*$ for sea ice. The large region $R_0$ assumes nothing about the microstructure. The small region $R_1$ inside assumes a brine volume of $p_2 = 0.12$; $f$ is frequency, $S$ is salinity, and $T$ is temperature.

crepancies may also be accounted for by uncertainties in the brine volume, which is discussed below.

Finally, Figures 5a, 5b, 6a, and 6b were created to be able to directly compare with *Arcone et al.* [1986, Figures 16 and 17], in which the real and imaginary parts of $\epsilon^*$ are plotted separately as a function of tem-

perature. The data shown in our figures are a representative set of the data from slabs 85-1, 85-2, and 85-3. These three slabs were chosen because their salinity values (before the experiment) were all close to each other, with $S = 4.8, 5.5$ and $5.4\ ^0/_{00}$, respectively. *Arcone et al.* [1986, Figures 16 and 17] plot data for ice which is
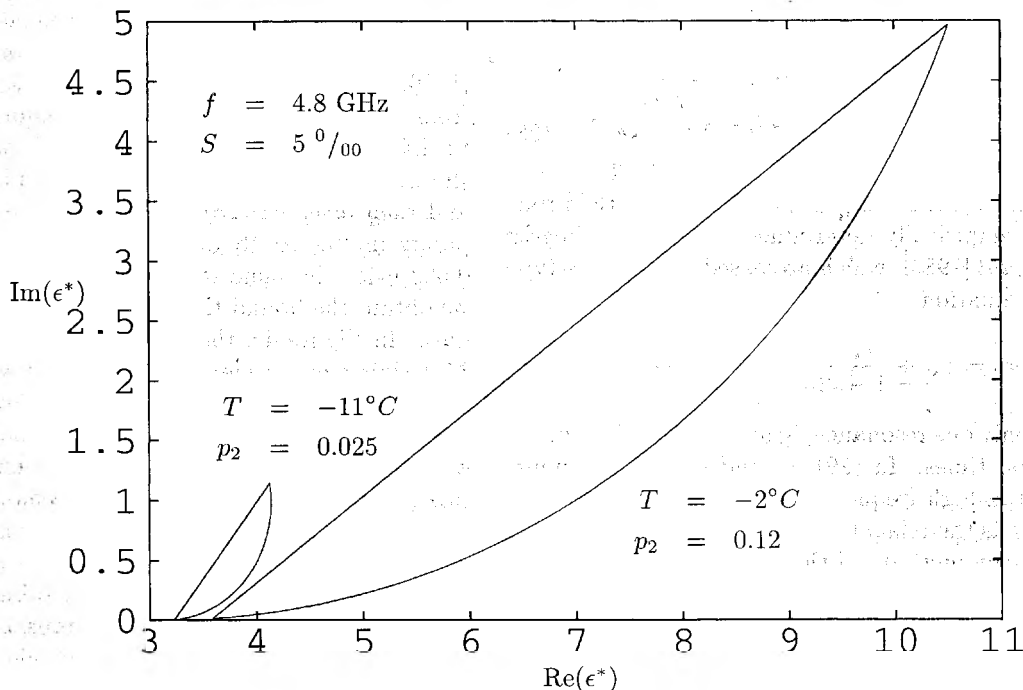
**Figure 2.** Bounds on $\epsilon^*$ for sea ice with different brine volumes $p_2$ or different temperatures $T$.

$$f = 4.8 \text{ GHz}$$
$$S = 5 \ ^0/_{00}$$
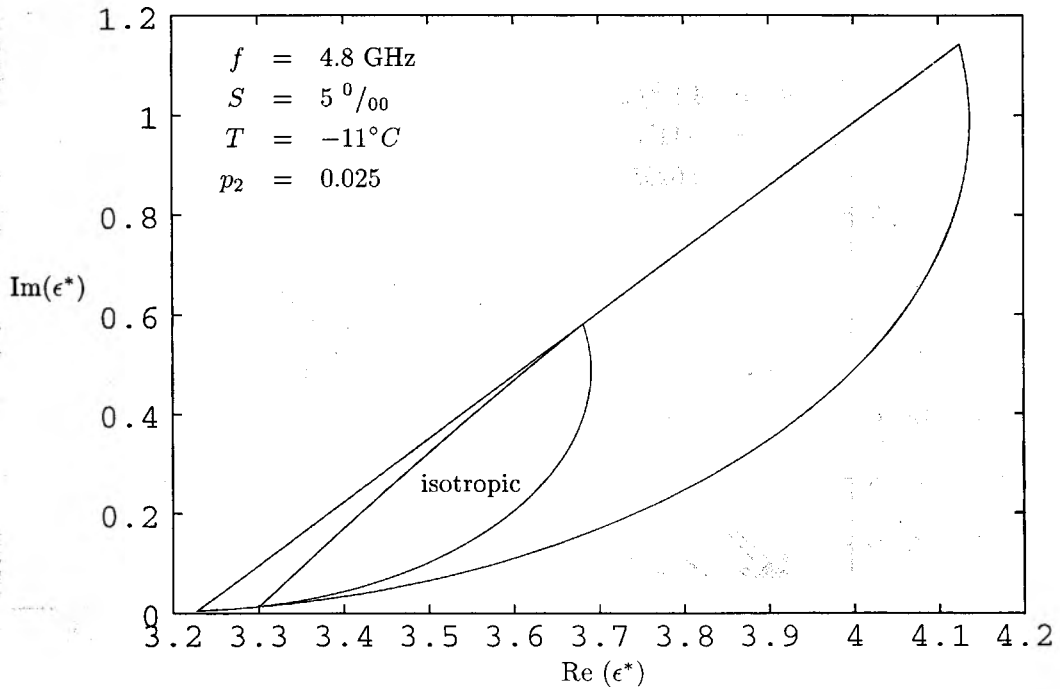$$T = -11°C$$
$$p_2 = 0.025$$

isotropic

**Figure 3.** Bounds on $\epsilon^*$ for given brine volume (outer bound $R_1$) and assuming isotropy within the horizontal plane (inner bound $R_2$).

warmed and subsequently cooled down. We only used the "warming" data, as once the ice has been warmed above $-5°C$, brine leaks out and air replaces some of the brine, which is reflected in the "cooling" data. For any given value of $T$, to create the upper and lower bounds shown in our figures, we first computed the $R_2$

bounds for that value of $T$ and with $S = 5 \ ^0/_{00}$. For a given value of $T$, the $R_2$ bound gives a maximum and minimum value for both $Re(\epsilon^*)$ and $Im(\epsilon^*)$ which corresponds to the coordinates of the vertices of $R_2$. The upper and lower bounds for any given $T$ shown in Figure 5a, for example, correspond to these maxi-
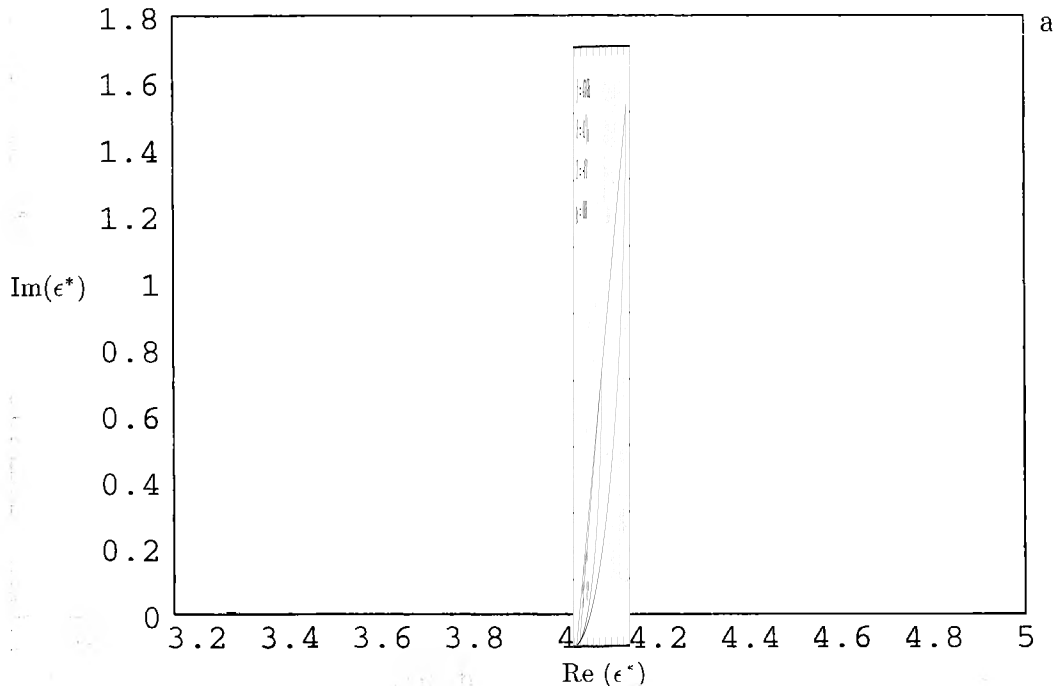


**Figure 4a.** Comparison of experimental data on $\epsilon^*$ with $R_1$ for given brine volume $p_2$ and with bound $R_2$ which assumes isotropy as well.

b

$f$ = 4.75 GHz
$S$ = 4.1 $^0/_{00}$
$T$ = $-11°C$
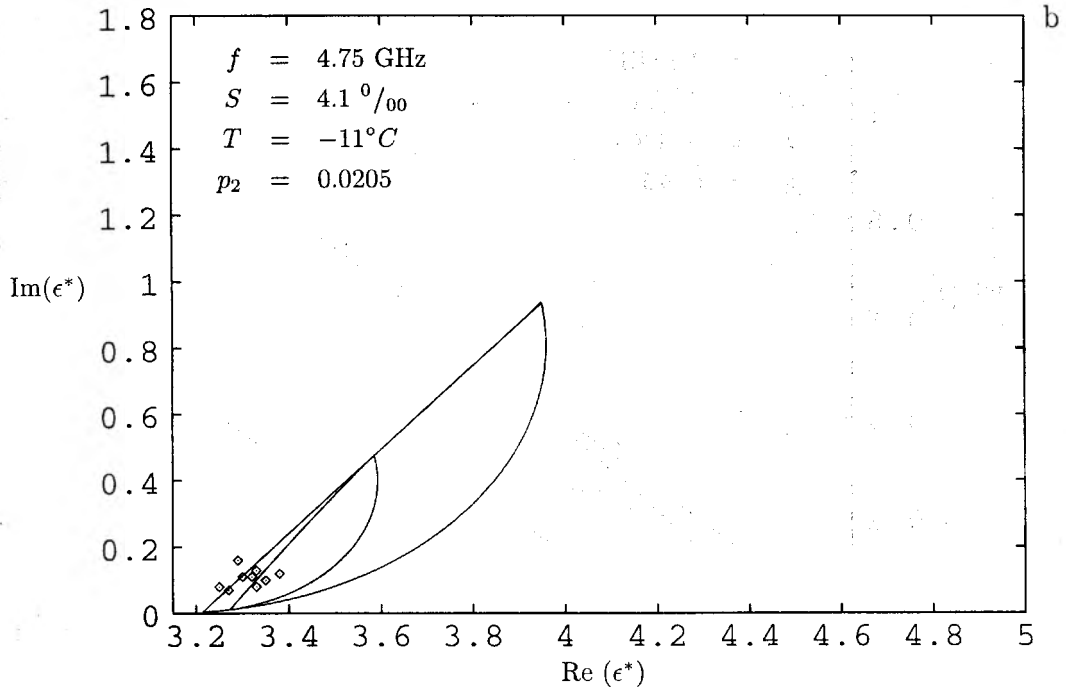$p_2$ = 0.0205

Im($\epsilon^*$)

Re ($\epsilon^*$)

**Figure 4b.** Same as Figure 4a, except for temperature of $-11°C$ and $p_2$ of 0.0205.

mum and minimum values of $Re(\epsilon^*)$ obtained from the vertices of $R_2$. Note that by considering $Re(\epsilon^*)$ and $Im(\epsilon^*)$ separately, it is easier for data points to lie inside the bounds, compared with plotting the points in the complex plane. More precisely, points which lie inside the bounds represented in Figures 5a, 5b, 6a, and 6b, if plotted in the complex $\epsilon^*$ plane, would only be required to lie in the corresponding rectangle (with

sides parallel to the axes) with two vertices matching the two vertices of $R_2$. Because of this added flexibility through plotting $Re(\epsilon^*)$ and $Im(\epsilon^*)$ separately, we found that we could obtain good fit with the data by using $R_2$ instead of $R_1$. We remark that the assumption of isotropy in the horizontal plane, which is implicit in constructing $R_2$, is fairly reasonable, as seen in the previous figures. Furthermore, since the sea ice was artifi-
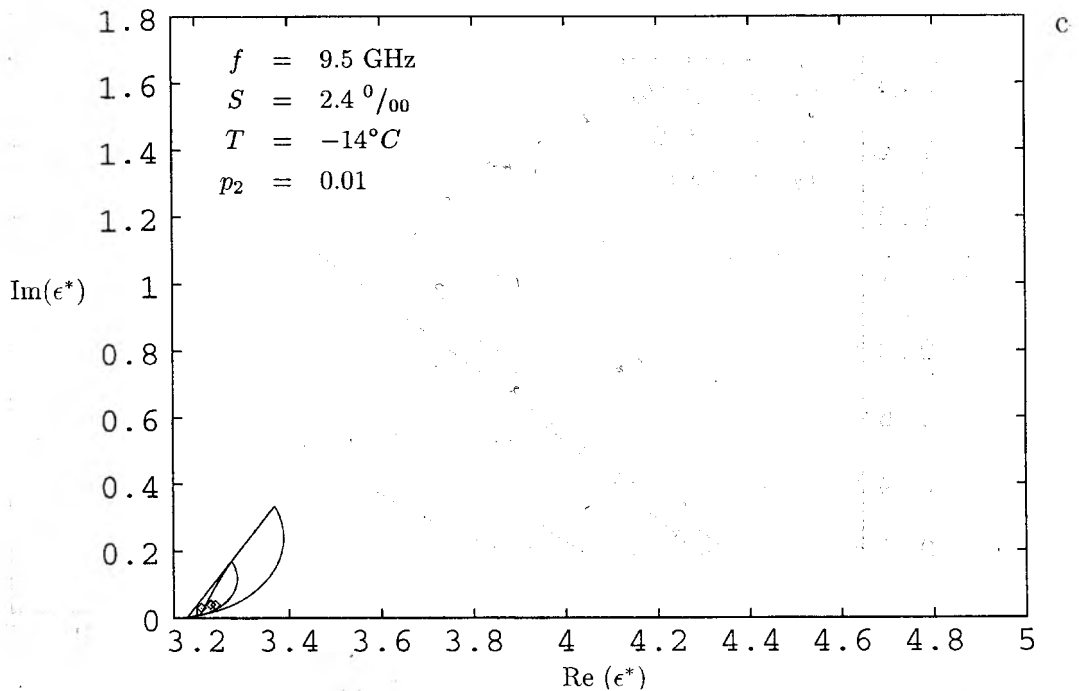
c

$f$ = 9.5 GHz
$S$ = 2.4 $^0/_{00}$
$T$ = $-14°C$
$p_2$ = 0.01

Im($\epsilon^*$)

Re ($\epsilon^*$)

**Figure 4c.** Same as Figure 4a, except for frequency of 9.5 GHz, salinity of 2.4$^0/_{00}$, temperature of $-14°C$, and $p_2$ of 0.01.
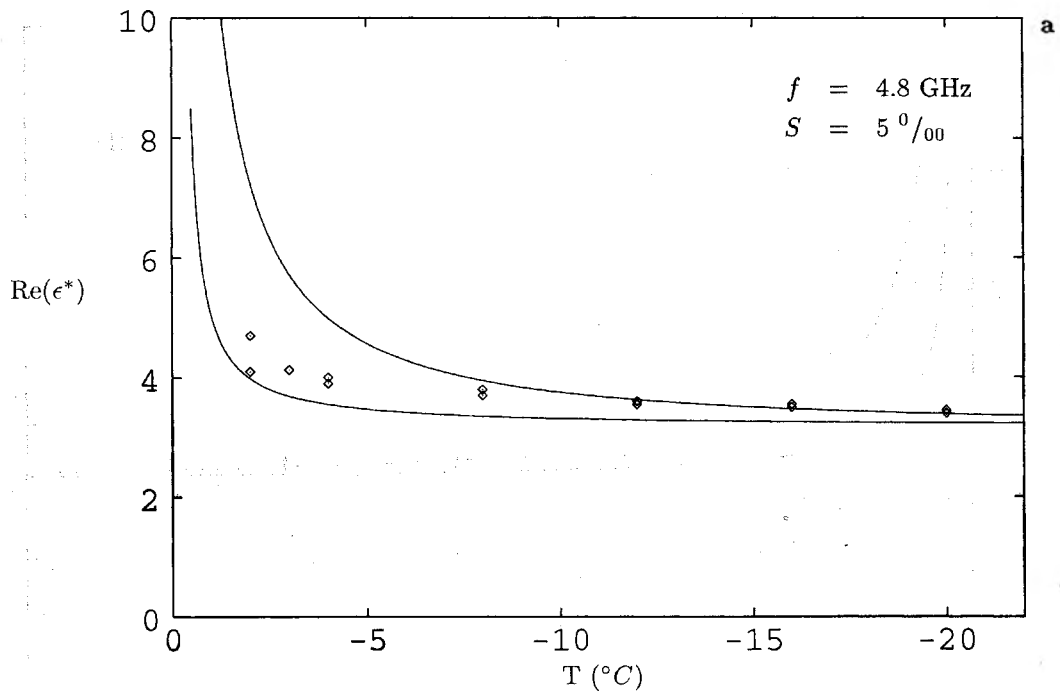
**Figure 5a.** Comparison of experimental data on $\epsilon^*$ with upper and lower bounds on $Re(\epsilon^*)$ obtained from $R_2$, as a function of temperature, at 4.8 GHz.

cially grown in an outdoor pool, where there is no well-developed, long-term current direction (which is usually present when the $c$ axis orientation of sea ice is highly anisotropic, as studied by *Cherepanov* [1971], *Weeks and Gow* [1980] and *Golden and Ackley* [1981]), we should not expect marked anisotropy in the data from *Arcone et al.* [1986].

## 5. Discussion

In comparing our bounds with the data of *Arcone et al.* [1986], we have found that perhaps the single most important quantity which determines the dielectric properties of sea ice is the brine volume $p_2$, and the regions $R_1$ and $R_2$ are very sensitive to this value. Un-
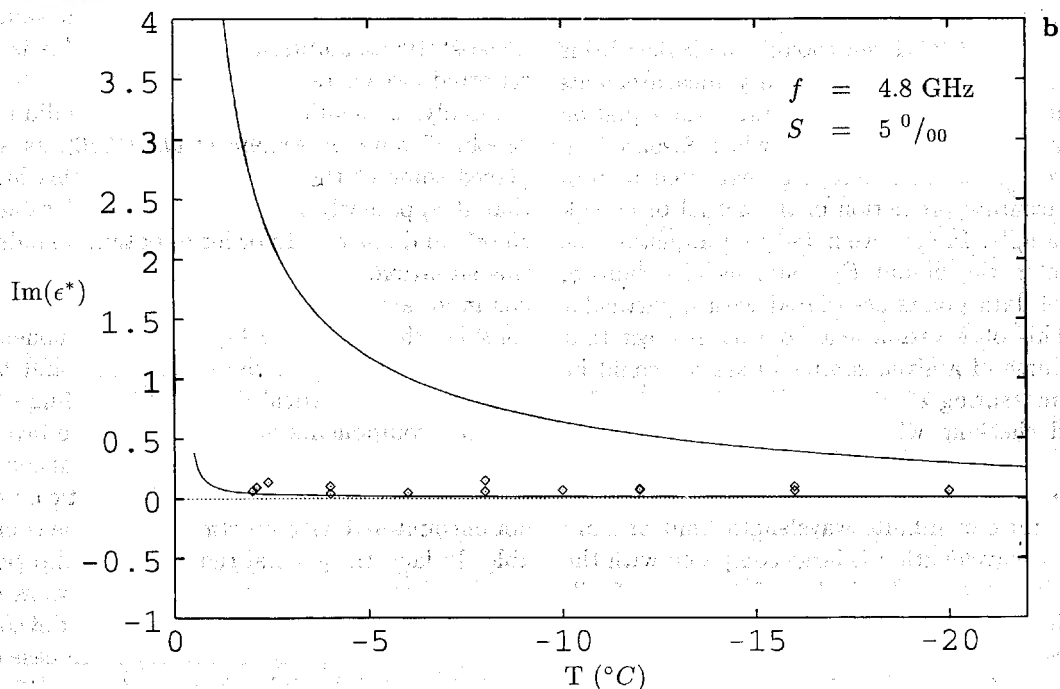


**Figure 5b.** Comparison of experimental data on $\epsilon^*$ with upper and lower bounds on $Im(\epsilon^*)$ obtained from $R_2$, as a function of temperature, at 4.8 GHz.
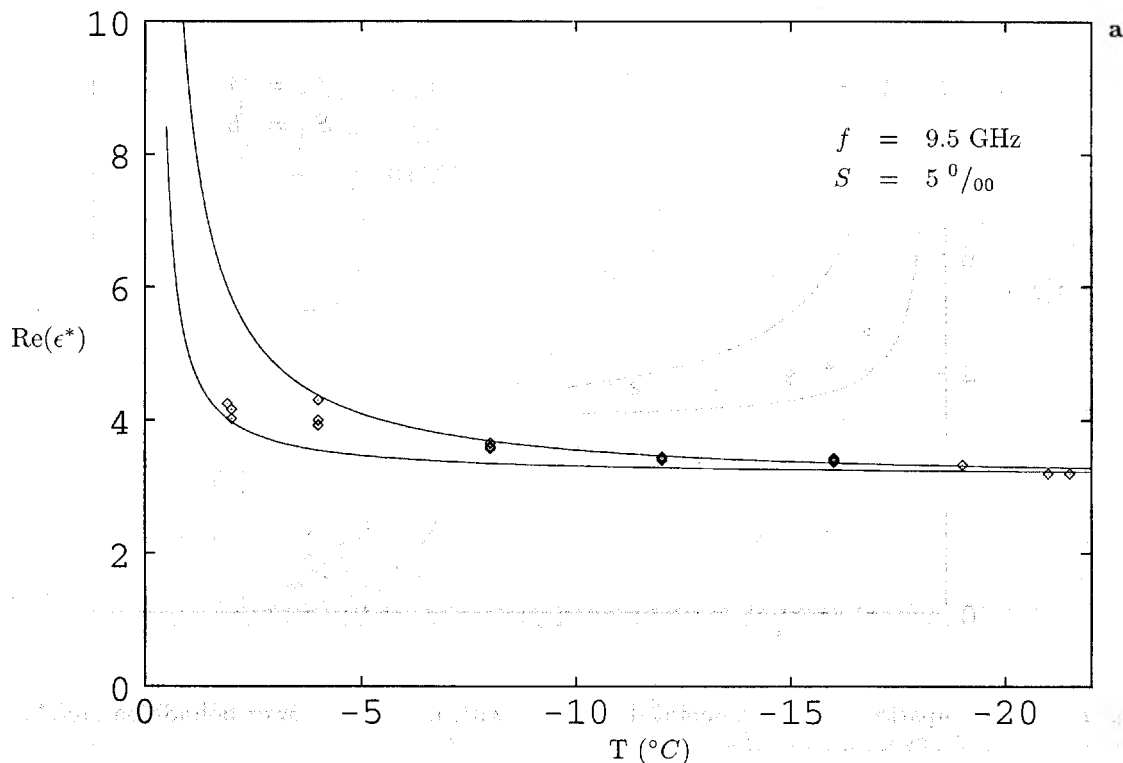
**Figure 6a.** Comparison of experimental data on $\epsilon^*$ with upper and lower bounds on $Re(\epsilon^*)$ obtained from $R_2$, as a function of temperature, at 9.5 GHz.

fortunately, the brine volume is quite difficult to measure experimentally. In comparing our bounds with the data, it appeared that the largest discrepancies occurred when there was the most uncertainty in the calculated value of the brine volume. As Arcone et. al. note, brine was leaking out of the slabs of sea ice until their temperature dropped below $-24°C$, and resumed again with $T$ between $-5°$ and $-6°C$. Even though the leaked brine was collected so that accurate salinity measurements could be made, under such circumstances the equation of *Frankenstein and Garner* [1967], which is based on theoretical considerations, cannot be expected to provide a very accurate prediction of the actual brine volume in the sample. In fact, we noted that adjusting the brine volume in the bound $R_1$ could usually capture any scatter of data points associated with a particular $S, T$ pair. This observation leads one to suspect that the brine volume of a given sample of sea ice could be deduced by measuring $\epsilon^*$ at a number of different frequencies and checking which brine volume yields the best correspondence between the bounds and the data.

As mentioned in section 2, the bounds are derived in the quasi–static or infinite wavelength limit and are valid when the wavelength $\lambda$ is large compared with the typical brine length scale $\beta$, which is of the order of millimeters. When $\lambda$ becomes comparable to $\beta$, we might expect that scattering effects become more significant. In this case we would expect that measured values of $Im(\epsilon^*)$ should be higher than those predicted by the bounds due to scattering losses. For the current fre-

quencies of 4.8 and 9.5 GHz we have found no evidence of any systematic offset of the experimental values when compared with the bounds. We conclude then that at these frequencies, scattering losses are minimal. In current work with S. Ackley and V. Lytle, we are comparing the quasi-static bounds with higher–frequency data, over a range of 26.5–40.0 GHz, where the validity of the quasi-static assumption is uncertain. This work will be reported elsewhere.

Finally, as mentioned in section 4, we did not use the "cooling" data of *Arcone et al.* [1986], as air has replaced some of the brine. The effect this has on $\epsilon^*$ is that it apparently lowers the measured values of both $Re(\epsilon^*)$ and $Im(\epsilon^*)$. In order to obtain bounds to model this situation, as well as multiyear ice which generally has more air volume than does first year ice, we must consider the sea ice to be a three-component random medium consisting of pure ice, brine, and air. However, the mathematical theory of bounding $\epsilon^*$ for three or more components is quite a bit more involved than for two, and involves the theory of several complex variables in which there arise new mathematical phenomena not encountered with functions of a single complex variable. In fact, the general theory of complex bounds was restricted to two components until the work of *Golden and Papanicolaou* [1985], and the first set of comprehensive bounds on $\epsilon^*$ in the multicomponent case was found by *Golden* [1986]. Subsequently, *Milton* [1987a,b] improved Golden's bounds and significantly extended the bounding theory. In subsequent work we would like to
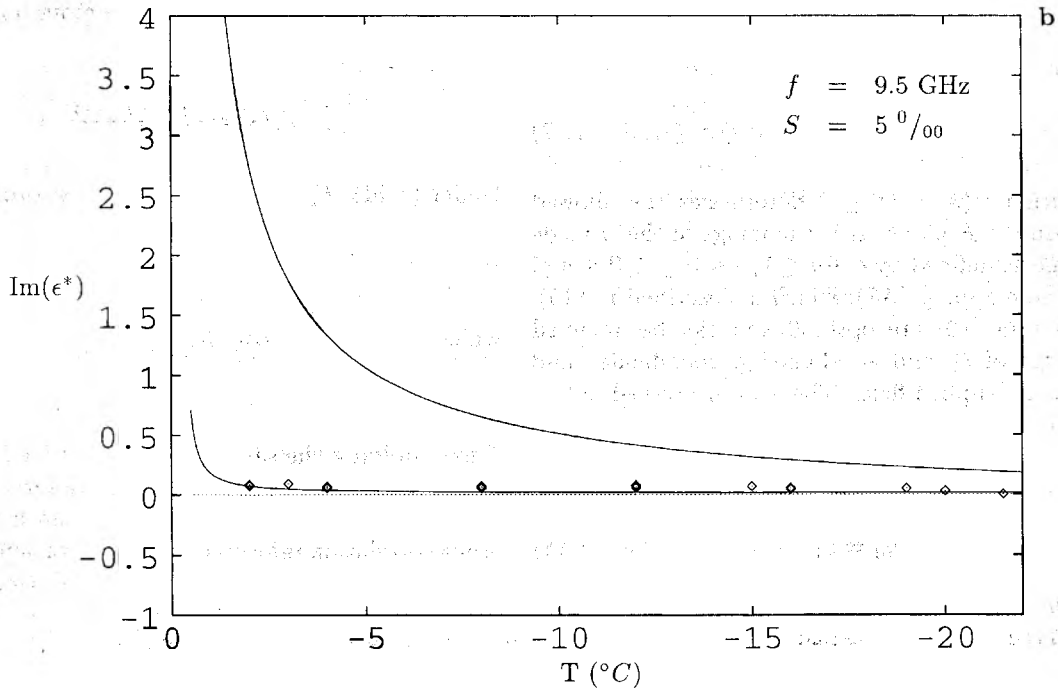
**Figure 6b.** Comparison of experimental data on $\epsilon^*$ with upper and lower bounds on $Im(\epsilon^*)$ obtained from $R_2$, as a function of temperature, at 9.5 GHz.

apply the Golden–Milton bounds to three–component sea ice.

## Appendix: The Analytic Continuation Method

Here we describe in more detail following *Golden* [1986], how the bounds $R_0$, $R_1$, and $R_2$ are obtained. We begin with the fundamental representation formula presented in section 2,

$$F(s) = \int_0^1 \frac{d\mu(z)}{s-z}, \qquad (A1)$$

where

$$F = 1 - \epsilon^*/\epsilon_2, \quad s = 1/(1 - \epsilon_1/\epsilon_2), \qquad (A2)$$

and $\mu$ is a positive measure on [0,1]. An alternative operator representation for $F(s)$ can be obtained from manipulation of (2)–(5),

$$F(s) = < \chi_1[(s + \Gamma\chi_1)^{-1}\mathbf{e}_k] \cdot \mathbf{e}_k >, \qquad (A3)$$

where $\Gamma = \nabla(-\Delta)^{-1}\nabla\cdot$. In the Hilbert space $L^2(\Omega)$ with $\chi_1$ in the inner product, $\Gamma\chi_1$ is a bounded self–adjoint operator of norm less than or equal to one. The integral representation (A1) is the spectral representation of the resolvent $(s+\Gamma\chi_1)^{-1}$, where $\mu$ is the spectral measure of the family of projections of $\Gamma\chi_1$, which provides a proof of (A1). We then see explicitly how $\mu$ depends on the geometry through $\chi_1$. Another proof of (A1) exploits the Herglotz property of $F(s)$.

Now we describe how (A3) can be used to inject geometrical information into the measure $\mu$. First, for $|s| > 1$, (A1) can be expanded about a homogeneous medium ($s = \infty$ or $h = 1$),

$$F(s) = \frac{\mu_0}{s} + \frac{\mu_1}{s^2} + \dots, \quad \mu_n = \int_0^1 z^n d\mu(z). \qquad (A4)$$

This is equivalent to a Taylor series expansion of $m(h) = \epsilon^*/\epsilon_2(\epsilon_1/\epsilon_2)$ around $h = 1$. Equating (A4) to the same expansion of (A3) yields

$$\mu_n = (-1)^n < \chi_1[(\Gamma\chi_1)^n\mathbf{e}_k] \cdot \mathbf{e}_k > . \qquad (A5)$$

It is through this moment formula that correlation information about the geometry is injected into the integral representation. If all the moments $\mu_n$ are known, then the measure $\mu$ is uniquely determined. Then (A1) provides the analytic continuation of the power series in (A4) to its full domain of analyticity, which is the full complex $s$ plane excluding [0,1].

Bounds on $\epsilon^*$ are obtained from (A1) as follows. First we describe how $R_0$ is obtained. By (A5), $\mu_0$ equals $p_1$, the volume fraction of medium 1. Then

$$0 \leq \mu_0 \leq 1. \qquad (A6)$$

For $s \in \mathbb{C}\backslash[0,1]$, where $\mathbb{C}$ is the complex plane, $F(s,\mu)$ in (A1) is a linear functional from the set $M$ of positive measures of mass $\leq 1$ on [0,1] into $\mathbb{C}$. Now $M$ is a compact, convex set of measures. The extreme points (or boundary) of the range of values of $F(s,\mu)$ in $\mathbb{C}$ are attained by one–point (Dirac) measures $\alpha\delta_a, 0 \leq \alpha \leq$

$1, 0 \leq a \leq 1$, since they are the extreme points of $M$. For these measures (which are so–called "$\delta$ functions"), $F$ has the form

$$F(s) = \frac{\alpha}{s - a}, \quad 0 \leq \alpha \leq 1, \quad 0 \leq a \leq 1. \quad (A7)$$

The condition $F(s = 1) \leq 1$ determines the allowed region $R_0$ in the $F$ plane. It is the image of the triangle in $(\alpha, a)$ space, defined by $\alpha + a \leq 1, 0 \leq \alpha \leq 1, 0 \leq a \leq 1$, under the mapping (A7), which is described in (15). The bounds in (15) are optimal and can be attained by laminates of $\epsilon_1$ and $\epsilon_2$ aligned perpendicular and parallel to the applied field. The arcs are traced out as the volume fraction varies.

If the volume fractions $p_1$ and $p_2 = 1 - p_1$ are fixed as well as $s$, then $\mu_0$ is fixed, with

$$\mu_0 = p_1. \quad (A8)$$

Then applying a similar extremal analysis as above shows that the values of $F$ lie inside the circle parametrized by

$$C_1(z) = \frac{p_1}{s - z}, \quad -\infty \leq z \leq \infty. \quad (A9)$$

On the other hand,

$$E(s) = 1 - \epsilon_1/\epsilon^* = \frac{1 - sF(s)}{s[1 - F(s)]} \quad (A10)$$

is also a Herglotz function like $F(s)$ and has a representation

$$E(s) = \int_0^1 \frac{d\nu(z)}{s - z}. \quad (A11)$$

Expansion of $E(s)$ yields $\nu_0 = p_2$, so that the values of $E$ lie inside the circle

$$\hat{C}_1(z) = \frac{p_2}{s - z}, \quad -\infty \leq z \leq \infty. \quad (A12)$$

In the $\epsilon^*$ plane the intersection $R_1$ of these two regions is bounded by two circular arcs corresponding to $0 \leq z \leq p_2$ in (A9) and $0 \leq z \leq p_1$ in (A12). These bounds are optimal and can be attained by a composite of uniformly aligned spheroids of material 1 in all sizes coated with confocal shells of material 2, and vice versa. These arcs are traced out as the aspect ratio varies.

If the material is further assumed to be statistically isotropic, then

$$\mu_1 = \frac{p_1 p_2}{d}, \quad (A13)$$

so that in view of (A4), $F$ is known to second order,

$$F(s) = \frac{p_1}{s} + \frac{p_1 p_2/d}{s^2} + \dots. \quad (A14)$$

A convenient way of including this information is to use the transformation of *Bergman* [1982],

$$F_1(s) = \frac{1}{p_1} - \frac{1}{sF(s)}. \quad (A15)$$

The function $F_1(s)$ is, again, a Herglotz function which has the representation

$$F_1(s) = \int_0^1 \frac{d\mu^1(z)}{s - z}. \quad (A16)$$

Under (A14), $F_1$ is known only to first order

$$F_1(s) = \frac{p_2/p_1 d}{s} + \dots, \quad (A17)$$

which forces the zeroth moment $\mu_0^1$ of $\mu^1$ to be

$$\mu_0^1 = p_2/p_1 d. \quad (A18)$$

Then applying the same procedure as for $R_1$ yields the bound $R_2$, where the boundaries are circular arcs parameterized by (25) and (26). We remark that higher–order correlation information can be conveniently incorporated by iterating (A15), as done by *Golden* [1986].

# References

Addison, J., Electrical properties of saline ice, *J. Appl. Phys.*, *40*, 3105–3114, 1969.

Arcone, S. A., A. J. Gow, and S. McGrew, Structure and dielectric properties at 4.8 and 9.5 GHz of saline ice, *J. Geophys. Res.*, *91*, 14,281–14,303, 1986.

Bergman, D. J., The dielectric constant of a composite material–A problem in classical physics, *Phys. Rep. C*, *43*, 377–407, 1978.

Bergman, D. J., Exactly solvable microscopic geometries and rigorous bounds for the complex dielectric constant of a two-component composite material, *Phys. Rev. Lett.*, *44*, 1285, 1980.

Bergman, D. J., Rigorous bounds for the complex dielectric constant of a two–component composite, *Ann. Phys.*, *138*, 78, 1982.

Berlyand, L., and K. Golden, Exact result for the effective conductivity of a continuum percolation model, *Phys. Rev. B, Condensed Matter*, *50*, 2114–2117, 1994.

Bruno, O., The effective conductivity of strongly heterogeneous composites, *Proc. R. Soc. London A*, *433*, 353–381, 1991.

Cherepanov, N. V., Spatial arrangement of sea ice

crystyal structure, *Probl. Arkt. Antark.*, *38*, 137–140, 1971.

Frankenstein, G., and R. Garner, Equations for determining the brine volume of sea ice from −0.5° to −22.9° C, *J. Glaciol.*, *6*, 943–944, 1967.

Golden, K., Bounds on the complex permittivity of a multicomponent material, *J. Mech. Phys. Solids*, *34*, 333–358, 1986.

Golden, K., Convexity and exponent inequalities for conduction near percolation, *Phys. Rev. Lett.*, *65*, 2923–2926, 1990.

Golden, K., Exponent inequalities for the bulk conductivity of a hierarchical model, *Commun. Math. Phys*, *43*, 467–499, 1992.

Golden, K., Scaling law for conduction in partially connected systems, *Proceedings of ETOPIM '93, Physica A.*, *207*, 213–218, 1994.

Golden, K. M., and S. F. Ackley, Modeling of anisotropic electromagnetic reflection from sea ice, *J. Geophys. Res.*, *86*, 8107–8116, 1981.

Golden, K., and G. Papanicolaou, Bounds for effective parameters of heterogeneous media by analytic continuation, *Comm. Math. Phys.*, *90*, 473–491, 1983.

Golden, K., and G. Papanicolaou, Bounds for effective parameters of multicomponent media by analytic continuation, *J. Stat. Phys.*, *40*, 655–667, 1985.

Hashin, Z., and S. Shtrikman, A variational approach to the theory of effective magnetic permeability of multiphase materials, *J. Appl. Phys.*, *33*, 3125–3131, 1962.

Hoekstra, P., and P. Capillino, Dielectric properties of sea and sodium chloride ice at UHF and microwave frequencies, *J. Geophys. Res.*, *76*, 4922–4931, 1971.

Kovacs, A., and R. M. Morey, Radar anisotropy of sea ice due to preferred azimuthal orientation of the horizontal c-axis of ice crystals, *J. Geophys. Res.*, *83*, 6037–6046, 1978.

Kozlov, S. M., Geometric aspects of homogenization, *Russ. Math. Surv.*, *44*, 91, 1989.

Mätzler, C., and U. Wegmüller, Dielectric properties of fresh–water ice at microwave frequencies, *J. Phys. D Appl. Phys.*, *20*, 1623–1630, 1987.

Milton, G. W., Theoretical studies of the transport properties of inhomogeneous media, Technical Report Physics IV, Dept. of Theor. Phys., Univ. of Sydney, 1979.

Milton, G. W., Bounds on the complex permittivity of a two-component composite material, *J. Appl. Phys.*, *52*, 5286–5293, 1981.

Milton, G. W., Multicomponent composites, electrical networks and new types of continued fractions I, *Comm. Math. Phys.*, *111*, 281–327, 1987a.

Milton, G. W., Multicomponent composites, electrical networks and new types of continued fractions II, *Comm. Math. Phys.*, *111*, 329–372, 1987b.

Milton, G. W., and K. Golden, Thermal conduction in composites, in *Thermal Conductivity 18*, edited by T. Ashworth and D. R. Smith, pp. 571–582, Plenum Press, New York, 1985.

Sihvola, A. H., and J. A. Kong, Effective permittivity of dielectric mixtures, *IEEE Trans. Geosci. Remote Sensing*, *26*, 420–429, 1988.

Stogryn, A., An analysis of the tensor dielectric constant of sea ice at microwave frquencies, *IEEE Trans. Geosci. Remote Sensing*, *GE-25*, 147–158, 1985.

Stogryn, A., and G. J. Desargant, The dielectric properties of brine in sea ice at microwave frequencies, *IEEE Trans. Antennas Propag.*, *AP-33*, 523–532, 1985.

Tinga, W. R., A. G. Voss, and D. F. Blossey, Generalized approach to multiphase dielectric mixture theory, *J. Appl. Phys.*, *44*, 3897–3902, 1973.

Vant, M. R., R. O. Ramseier, and V. Makios, The complex-dielectric constant of sea ice at frequencies in the range 0.1–40 GHz, *J. Appl. Phys.*, *49*, 1264–1280, 1978.

Weeks, W. F., and S. F. Ackley, The growth, structure and properties of sea ice, *Cold Reg. Res. and Eng. Lab. Monogr. 82-1*, pp. 130, 1982.

Weeks, W. F., and A. J. Gow, Crystal alignments in the fast ice of Arctic Alaska, *J. Geophys. Res.*, *85*, 1137–1146, 1980.

K. Golden, Department of Mathematics, University of Utah, Salt Lake City, UT 84112.